Automatic identification of dense damage-sensitive features in civil infrastructure using sparse sensor networks

Automatic identification of dense damage-sensitive features in civil infrastructure using sparse sensor networks

Said Quqa[a,*], Luca Landi[a], Pier Paolo Diotallevi[a]

[a] *Department DICAM, University of Bologna, Viale del Risorgimento 2, 40136 Bologna, Italy*

ABSTRACT

Widespread monitoring of bridges is yet rarely employed at a territorial level due to the high costs of the monitoring systems. However, the aging of civil infrastructures, combined with the growing traffic demand, poses the need for a simple and automatic tool that helps emergency management. In this paper, an integrated algorithm for the identification of dynamic and dense quasi-static structural features exploiting moving vehicles is proposed. Filtering raw acceleration structural responses, triggered by passing vehicles, enables the identification of modal parameters and curvature influence lines. The procedure can be implemented efficiently as the main computational core consists of convolutions. The definition of a curvature-based damage index leads to accurate localization and quantification of structural anomalies using few sensors. The proposed procedure is tested on three viaducts of the Italian A24 motorway. Moreover, a numerical model is studied to evaluate the potentialities of the strategy for damage localization.

KEYWORDS: Structural health monitoring, modal identification, influence line, non-stationary, vehicular traffic, damage quantification.

Declaration of interests: none.

1. INTRODUCTION

Failure in road infrastructure leads to immediate direct losses due to the costs of repair or demolition/reconstruction, as well as long-term indirect effects, involving the costs of temporary measures for emergency management, traffic delays, deviations, and accidents, which may also entail longer journeys for emergency vehicles. Economic losses on industry and local business, as well as the consequent decrease of demand for work, complete the framework of a catastrophic event, which can also involve the most severe loss concerning human life. Due to the aging of bridges and viaducts and the evolution of traffic demand, structural degradation is becoming a serious matter of concern. Due to the general lack of resources, the recent trend is to migrate from the traditional planned maintenance to condition-based maintenance, performed when certain indicators show signs of decreasing performance or upcoming failure. In this way, the uneconomical "fail and fix" approach is going to be replaced by a more efficient "prevent and predict" strategy. In the last decades, structural health monitoring (SHM) systems have

[*] Correspondence to: Said Quqa, Department DICAM, University of Bologna, Viale Risorgimento 2, 40136 Bologna, Italy, e-mail: said.quqa2@unibo.it
E-mail addresses: said.quqa2@unibo.it (S. Quqa), l.landi@unibo.it (L. Landi), pierpaolo.diotallevi@unibo.it (P.P. Diotallevi).

proven to provide a valuable tool to decision-makers in order to optimize maintenance or interrupt the ordinary use of crumbling infrastructure. Although "information never hurts" [1], the high cost of traditional monitoring systems makes the infrastructure owners skeptical about the investment [2,3]. Indeed, the age of most civil infrastructure would require the widespread deployment of monitoring systems to manage interventions at a territorial scale, thus involving considerable expenses, which are generally unjustified for minor infrastructures.

Due to the accessible cost of the components employed in wireless sensor networks (WSNs) and the development of power-optimized systems [4], dense distributions of smart nodes are increasingly used for SHM applications, involving however issues in managing and synchronizing large data volumes. Several structural identification algorithms tailored for WSNs have thus been proposed, introducing decentralized strategies for data management and feature computing. Quqa et al. [5] recently proposed a decentralized algorithm for the identification of instantaneous modal parameters based on clustered filter banks (CBFs), enabling near real-time applications using star-topology networks. Based on the same principle, the modal assurance distribution (MAD), a novel time-frequency representation of multivariate signals, was presented to decouple modal contributions which are mixed in the structural response and identify real-time damage sensitive features of strongly time-varying structures [6]. This algorithm has shown superior performance when compared to the widely used empirical mode decomposition (EMD), even when dealing with non-linear structures [7]. Accurate identification results have also been obtained under several types of input excitation.

Although vehicular traffic is an important source of excitation that allows collecting recordings with a high signal-to-noise ratio compared to ambient vibration, the time-variability of the load may not comply with the assumption of stationary vibration at the base of most operational modal analysis (OMA) techniques [8]. The passage of weighting loads may also modify the short-time behavior of the structure, opening breathing cracks in reinforced concrete (RC) elements and producing localized dynamic effects when vehicles hit the expansion joints. Recordings that contain such effects are generally discarded in OMA procedures, whilst they may be representative of the structural state. Moreover, the spatial information inherent in the structural response collected under moving loads may disclose valuable structural features for SHM purposes. Aloisio et al. recently studied RC viaducts using signals collected under moving loads to identify their elastic moduli [9]. Khan et al. recently used traffic-induced vibration to identify scour in a decentralized fashion [10]. In the last years, drive-by monitoring, i.e., using data collected by sensors deployed on moving vehicles, has gained growing interest among the research community [11]. Yang et al. conducted pioneering studies about extracting bridge frequencies from the response of a passing vehicle, thus introducing the concept of "drive-by monitoring" [12], while González et al. managed to identify the damping ratio [13] using the same approach. Also, Aloisio et al. [14] used the response of a passing instrumented vehicle to identify the bending stiffness of the same viaducts studied in [9]. Besides, other measuring devices, e.g., video cameras [15] and weigh-in-motion systems [16] were considered in the literature to infer information about the moving loads, and advanced SHM strategies exploiting sensors placed both on the structure and on the moving vehicles have been developed to better describe the vehicle-bridge interaction [17].

Recent studies have been devoted to identifying dense structural features (i.e., describing the structural behavior at a large number of locations) by analyzing the quasi-static effects due to moving loads. He et al. proposed a damage identification approach that is able to quantify damage using displacement data collected by a sensor moving at low speed, thus only collecting the quasi-static response of the specimen [18]. Cavedas et al. assessed the performances of moving principal component analysis (MPCA) and robust regression analysis (RRA) for this purpose using both displacement and rotation measurements [19]. Other techniques attempt to obtain similar results by analyzing recordings collected by sensors deployed on the bridge rather than on moving vehicles, which are generally less sensitive to vehicle-bridge interaction effects. Frøseth et al. proposed an efficient formulation to calculate the displacement influence line of the structure through deconvolution in the frequency domain [20]. However, in this technique, loads must be known in advance. In the time domain, Zheng et al. presented an efficient regularized least-squares-based

method for the identification of influence lines using multi-axle vehicle excitation [21]. A review of the most recent methods employing both frequency- and time-based models and an in-depth comparison are presented in [22]. Hester et al. employed the rotation measurements collected at the extrema of a beam to identify and localize damage accurately [23]. Besides rotations and displacement, strain measurements have also been largely employed [24–26]. However, accelerometers, which are still the most widely used sensors in SHM, have rarely been used for the identification of quasi-static structural features due to problems related to the recording of low-frequency components. Nevertheless, recent MEMS technologies, as well as more conventional force-balanced accelerometers (FBA), enable the acquisition of low-frequency vibration down to DC and can thus be exploited for this purpose.
The aim of this paper is threefold:

1) Demonstrate the applicability of the MAD, already proposed in [6] for long-term applications, to civil infrastructures subjected to moving loads. Although the MAD-based identification algorithm has proven to have several benefits over other literature methods (e.g., the automatic identification and extraction of instantaneous modal features even in the presence of narrow-band disturbances [6] and non-linear effects [7]) in several scenarios, moving loads and short signal windows pose a further challenge which needs to be addressed to propose an effective SHM strategy for operating civil infrastructure.
2) Propose a unified and automatic identification strategy for estimating both dense quasi-static structural features and modal parameters using sparse sensor networks (consisting of down to just one sensing device) collecting acceleration data. The procedure is based only on acceleration recordings, without the need for additional devices to track the vehicle location. Moreover, the algorithm proposed for automatic selection and processing of signal windows related to the vehicle passage make this method particularly suitable for crowdsourced cloud computing applications.
3) Test the potentialities of the identified quasi-static structural features for damage localization and quantification. Due to the physical meaning of the quasi-static feature studied in this paper, a curvature-based damage-sensitive feature (DSF) is proposed, removing the complex procedures (and thus approximations) which are generally necessary for traditional methods to calculate curvature from identified mode shapes. The use of this novel approach brings considerable advantages, as it enables accurate localization of structural anomalies using limited (and thus low-cost) instrumentation, suitable for widespread monitoring, and removes the need for data synchronization. Moreover, differently from most literature methods [27,28], the damage entity can be quantified without any knowledge on the structural masses and avoiding the use of finite element models.

The first two points are supported by the results obtained using the acceleration data collected on three viaducts of the Italian A24 motorway, analyzed in several works by Aloisio et al. [9,14,29,30]. Moreover, the results obtained for a numerical case study in different damage scenarios are reported to show the potentialities of the proposed method for damage detection, localization, and quantification.

2. STRUCTURAL IDENTIFICATION UNDER MOVING LOADS

Isostatic schemes, such as simply supported beams, are typically considered for the design of RC bridges and viaducts due to their capacity to accommodate the expansion (or contraction) effects of environmental loads, such as temperature, that would instead generate unwanted stress states in hyperstatic structures. In this study, the simply supported beam will be considered as representative of a span of common RC viaducts.
Literature in the field of SHM reports several cases where the effectiveness of dynamic identification methods is affected by structural nonlinearities [31]. Moreover, in civil structures, damage is often related to an increment in the degree of nonlinearity [32]. However, material and geometrical nonlinearities, as well as those related to the boundary conditions, are generally activated by significant displacements. Since

the method proposed in this paper is conceived for ordinary traffic loads, it is assumed that the structure is subjected to small displacements and thus behaves linearly.
In general, the equation of motion of a linear simply supported beam with uniform cross-section subjected to a generic load function acting orthogonally to the axis of the structure $p(z,t)$ can be represented as

$$\mu \frac{\partial^2 u(z,t)}{\partial t^2} + d \frac{\partial u(z,t)}{\partial t} + EI \frac{\partial^4 u(z,t)}{\partial z^4} = p(z,t) \tag{1}$$

where μ is the mass per unit length, d is a damping coefficient, and EI is the flexural stiffness, given by the elastic modulus of the material E and the inertia of the section I. In Eq. (1), $u(z,t)$ is a function in space (z) and time (t) that indicates the structural displacement response in the direction of the load, while the $\partial^d f/\partial x^d$ operator indicates the d-th derivative of the function f with respect to x. Using the superposition principle, the structural response can be written as a linear combination of modal responses

$$u(z,t) = \sum_{m=1}^{\infty} \phi_m(z) q_m(t) \tag{2}$$

where $\phi_m(z)$ is the m-th mode shape of the structure and $q_m(t)$ is a function of time that presents a peak in the frequency domain around the damped m-th circular frequency $\omega_{d,m}$ which, in the case of low damping, can be assumed as the m-th natural (circular) frequency of the structure

$$\omega_m = \frac{m^2 \pi^2}{l^2} \sqrt{\frac{EI}{\mu}} \tag{3}$$

where l is the length of the beam. In free vibration conditions, i.e., $p(z,t) = 0$, if damping is small, the structural response can be approximated as

$$u(z,t) = \sum_{m=1}^{\infty} c_m \sin\left(\frac{m\pi z}{l}\right) e^{-\xi \omega_m t} \sin(\omega_m t) \tag{4}$$

with c_m representing a constant depending on the initial conditions and ξ denoting the modal damping ratio, here assumed as equal for all the vibration modes.
Typically, in SHM applications, accelerometers are employed to collect the structural responses. The collected acceleration, in the case of free vibration, can be described using the following equation:

$$\frac{\partial^2 u(z,t)}{\partial t^2} = \sum_{m=1}^{\infty} c_m \sin\left(\frac{m\pi z}{l}\right) \ddot{q}_m(t) \tag{5}$$

where

$$\ddot{q}_m(t) = \omega_m^2 e^{-\xi \omega_m t} [(\xi^2 - 1) \sin(\omega_m t) - 2\xi \cos(\omega_m t)] \tag{6}$$

The Fourier transform of the acceleration can thus be calculated as

$$A_a(z,f) = \mathcal{F}\left[\frac{\partial^2 u(z,t)}{\partial t^2}\right] = \sum_{m=1}^{\infty} c_m \sin\left(\frac{m\pi z}{l}\right) Q_m(f) \tag{7}$$

with $Q_m(f)$ representing a normalized transfer function of the single degree of freedom (SDOF) system associated with the m-th mode:

$$Q_m(f) = \frac{\omega_m^3(1+\xi^2) + 4j\pi\xi\omega_m^2 f}{\omega_m^2 + (\xi\omega_m + 2j\pi f)^2} \tag{8}$$

Considering now a single moving load of magnitude P with constant speed v and negligible mass, the load function can be written as $p(z,t) = P\delta(z - vt)$ and, if damping is small, the displacement response of the structure becomes [33]:

$$u(z,t) = \frac{Pl^3}{48EI} \sum_{m=1}^{\infty} \frac{1}{m^2(m^2-\alpha^2)} \sin\left(\frac{m\pi z}{l}\right) \left[\lambda_m(t) - \frac{\alpha}{m} e^{-\xi\omega_m t} \sin(\omega_m t)\right] \tag{9}$$

with

$$\alpha = \frac{vl}{\pi}\sqrt{\frac{m}{EI}} \tag{10}$$

$$\lambda_m(t) = \sin\left(\frac{m\pi v t}{l}\right) \prod\left(\frac{vt}{l} - \frac{1}{2}\right) \tag{11}$$

where $\prod(t)$ is a rectangular function used to limit the support of $\lambda_m(t)$ to the interval $t \in [0, l/v]$, i.e., when the load is on the beam, and δ denotes the Dirac delta function. The acceleration response, obtained by double derivative thus reads:

$$\frac{\partial^2 u(z,t)}{\partial t^2} = -\frac{Pl^3}{48EI} \sum_{m=1}^{\infty} \frac{1}{m^2(m^2-\alpha^2)} \sin\left(\frac{m\pi z}{l}\right) \left\{\left(\frac{m\pi v}{l}\right)^2 \lambda_m(t) + \frac{\alpha}{m} \ddot{q}_m(t)\right\} \tag{12}$$

and its Fourier transform is

$$A_v(z,f) = \mathcal{F}\left[\frac{\partial^2 u(z,t)}{\partial t^2}\right] = -\frac{Pl^3}{48EI} \sum_{m=1}^{\infty} \frac{1}{m^2(m^2-\alpha^2)} \sin\left(\frac{m\pi z}{l}\right) \left[L_m(f) - \frac{\alpha}{m} Q_m(f)\right] \tag{13}$$

where $L_m(f)$ is a function depending on the quasi-static effects of the moving load and has the following expression:

$$L_m(f) = \frac{\pi v m^3}{2l\left(\frac{l^2 f^2}{v^2} - \frac{m^2}{4}\right)} e^{j\pi\left(\frac{m-1}{2} - \frac{lf}{v}\right)} \sin\left(\frac{\pi l f}{v} - \frac{m\pi}{2}\right) \tag{14}$$

Comparing Eq. (7) and Eq. (13), it is possible to notice that, except for the constants, the second equation has an additional term represented by Eq. (14). The expression of $L_m(f)$ can be obtained by applying the modulation theorem to a sinc function, as shown in Appendix A. The resulting function presents a sharp peak at a frequency value that grows with m, assuming however lower magnitude. Also, $L_m(f)$ decreases

with f^2. It can be therefore be assumed that the term $L_m(f)$ has a non-negligible contribution in the structural response only in the low-frequency range. On the other hand, the function $Q_m(f)$ carries information about the m-th vibration mode of the structure, and thus it generally governs the medium-high-frequency content of the response spectrum.
Vehicular traffic, though as an ensemble of moving loads, induce manifold effects in the structural vibration response, namely (1) quasi-static effects due to the deflection of the structure under the weight of the passing vehicles, (2) dynamic effects due to instantaneous equilibrium between inertial, elastic, and dissipative forces, and (3) short-term effects, here addressed as "noise", mainly given by the interaction between the vehicle wheels and the uneven road surface. The first phenomenon, described in Eq. (14), is closely related to the instantaneous vehicle location and mainly affects the lowest (typically sub-hertz) frequency range in the spectrum of the structural response. The second family of effects can be modeled as the superposition of a set of structural vibration modes, described in Eq. (8), the first of which generally populate the frequency range between few hertz and few dozen hertz for the most common RC viaducts. Finally, noise affects the entire spectrum, with the majority of its energy concentrated at the higher frequencies.
Due to the particular structure of the response spectrum, different structural features can be analyzed by individually processing different frequency bands. In this paper, the attention is posed on the low-frequency range, with the aim of extracting quasi-static damage-sensitive features which depend on the location of the vehicle (i.e.., the influence line), as well as modal parameters (i.e., natural frequencies and sparse estimates of the mode shapes) of the first dominating dynamic contributions.
As shown in reference [6], the MAD can be used to build adaptive filter banks able to extract decoupled modal contributions from the structural response collected at different instrumented locations. In the mentioned study, critically sampled signal components were extracted using wavelet filter banks, with the aim of reducing the weight of identified parameters. Besides, if the structure can be modeled as a linear time-invariant (LTI) system, static filter banks can be employed, improving the efficiency of the identification procedure [5]. In this paper, the aforementioned concepts are employed in the structural identification of civil infrastructures under the following assumptions:

1) A vehicle is modeled as a single constant load, regardless of the spacing between the wheel axles;
2) Only one vehicle at a time passes through the bridge with a constant velocity;
3) The vehicle-bridge coupling effects are neglected.

The first two assumptions allow considering the loading function as $p(x,t) = P\delta(x - vt)$. If multiple axles are present, the suppression of certain frequency values in the response spectrum should be taken into account. However, in the following sections, it is shown that the first assumption can generally be legitimately considered. Moreover, due to the modest length of single spans in RC infrastructures, the second hypothesis can be generally assumed in the case of fluid traffic. Finally, concerning the third point, RC infrastructures are typically massive with respect to ordinary cars.
In the following sections, two identification approaches, based on the low-frequency and (medium-)high-frequency effects, respectively, are proposed to obtain different structural features which may be of particular interest for the assessment of the structural integrity.

2.1 Low-frequency effects

Applying a sub-hertz lowpass filter to the structural acceleration response collected at location distant ζl (with $\zeta < 1$) from the first support during the passage of a vehicle with constant velocity v, in the interval $t \in [0, l/v]$, from Eq. (12), it is possible to define

$$h^{(\zeta)}[t] = \left(\left. \frac{\partial^2 u(z,t)}{\partial t^2} \right|_{z=\zeta l} * \bar{b}_0 \right)[t] \cong -\frac{Pl^3}{48EI} \sum_{m=1}^{\gamma} \frac{\pi^2 v^2 \sin(m\pi\zeta)}{l^2(m^2 - \alpha^2)} \sin\left(\frac{m\pi v t}{l}\right) \tag{15}$$

where $*$ is the convolution operator, $\bar{b}_0[\tau]$ is the impulse response of the lowpass filter, and γ indicates a small number of contributions with the majority of their frequency content in the sub-hertz interval. Assuming the distance traveled by the vehicle as $z = vt$, it is possible to obtain a function of space which represents the double derivative of the displacement influence line of the structure with respect to space as:

$$h^{(\zeta)}[z] = \sum_{m=1}^{\gamma} h_m^{(\zeta)}[z] \cong \sum_{m=1}^{\gamma} -\frac{Pl^3}{48EI} \frac{\pi^2 v^2 \sin(m\pi\zeta)}{l^2(m^2-\alpha^2)} \sin\left(\frac{m\pi z}{l}\right) \tag{16}$$

$h^{(\zeta)}[z]$ is thus the influence line of the curvature of the beam in the normalized location ζ and is therefore also proportional to the influence line of the bending moment. Due to the Maxwell-Betti reciprocal work theorem, Eq. (16) can also be interpreted as the curvature of the deflection shape of the beam subjected to a force P statically applied at the instrumented location.

It should be noted that $h^{(\zeta)}[z]$ can be identified using a single sensing device deployed on the structure, offering however a dense description of the structural behavior, depending on the sampling frequency of the collected data. Moreover, the curvature is a well-established DSF that is typically obtained through double derivation upon identifying mode shapes through a set of limited sensors. The traditional approach generally involves the introduction of computational errors (e.g., due to the central difference method), which may affect the robustness of the outcomes in the presence of noisy identified parameters. Besides, the curvature is typically estimated only at the instrumented locations. Conversely, the proposed method exploits the collected acceleration to infer information about curvature in potentially continuous locations, without performing any approximations in the derivation process.

Considering loads consisting of two axles, an equivalent function in space can be obtained by calculating $h^{(\zeta)}[z] * \varepsilon_w[z]$, where $\varepsilon_w[z] = \delta[z] + \delta[z+w]$, w is the distance between the wheel axles and $\delta[z]$ is a discrete Dirac delta function, thus obtaining

$$h^{(\zeta)}[z] * \varepsilon_w[z] = h^{(\zeta)}[z] + h^{(\zeta)}[z+w] \tag{17}$$

Physically, this function represents the influence line of the curvature of the beam when the first load is at location z and the second is at location $z+w$. In the frequency domain, the spectrum of Eq. (17) can be obtained as a simple point-by-point product, i.e., $H^{(\zeta)}[f]E_w[f]$, where $H^{(\zeta)}[f]$ and $E_w[f]$ are the spectra of $h^{(\zeta)}[z]$ and $\varepsilon_w[z]$, respectively, reported in Fig. 1. Considering the frequency values $f_s^{(1)}$ and $\bar{f}_s$, defined as

$$f_s^{(1)} = \left(s + \frac{1}{2}\right)\frac{v}{l} \tag{18}$$

$$\bar{f}_s = \left(s - \frac{1}{2}\right)\frac{v}{w} \tag{19}$$

representing the s-th zeros of $H_1^{(\zeta)}[f]$ (i.e., the frequency spectrum of $h_1[z]$) and $E_w[f]$, respectively, it is possible to assume that $H^{(\zeta)}[f] \cong H^{(\zeta)}[f]E_w[f]$ if $f_1^{(1)}$"$\bar{f}_1$, i.e., if w "l. In particular, assuming the limit

$$\frac{f_1^{(1)}}{\bar{f}_1} = 3\frac{w}{l} \leq \frac{1}{3} \tag{20}$$

will guarantee that the double load affects $H^{(\zeta)}$ of up to 13%. As a geometrical limit, it can thus be posed that $l \geq 10w$. This condition can be generally assumed in the case of large civil infrastructures. However, the effect of multiple loads generally produces a smoother influence line. In the specific case of two axles,

this can be observed analytically since the effect of $E_w[f]$ is of reducing the higher perceptible contributions (with an m index close to γ) of $h^{(\zeta)}[z]$. Since higher-frequency contributions are attenuated, the resulting function in space is smoother.
In addition to the aforementioned geometrical constraints, the sampling frequency of the accelerometers should be selected based on the required resolution of the influence line. In particular, considering the vehicle velocity v and the required spatial resolution r, the minimum sampling frequency can be obtained as $f_s = v/r$ [34].

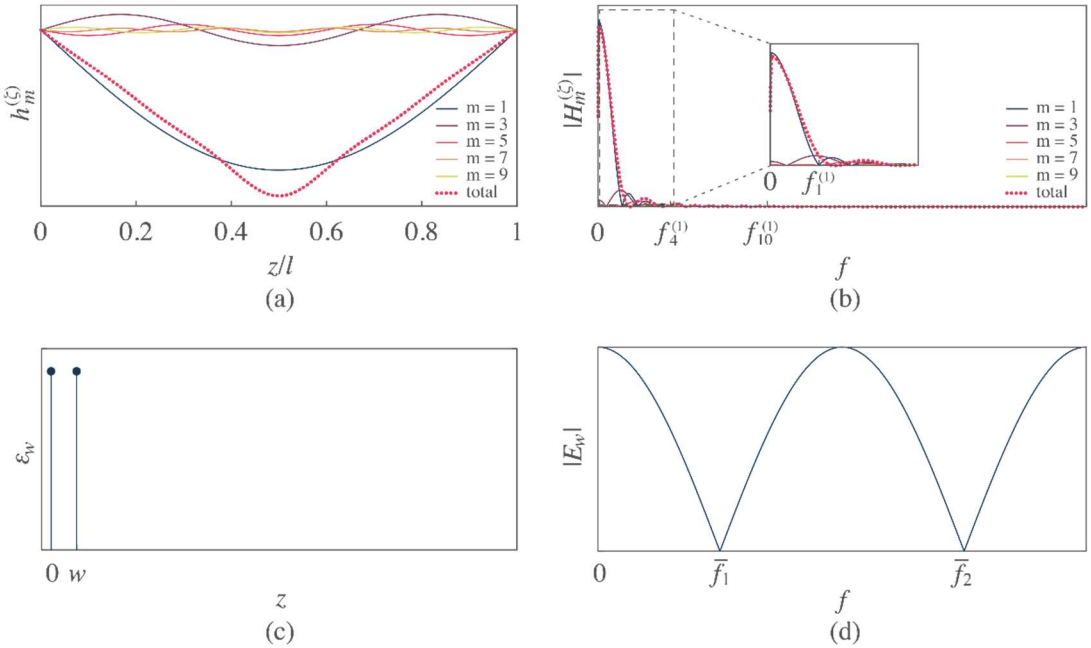

Fig. 1 – Quasi-static components of the structural response in space (a) and frequency domain (b); two-axle excitation in space (c) and frequency domain (d)

2.2 High-frequency effects

The high-frequency range of the response spectrum of the structure under a single moving load is analogous to the response spectrum obtained in free vibration condition, reported in Eq. (7). Here, each term of the summation is related to a different resonant frequency of the structure and presents a peak in the frequency domain around the frequency ω_m. Assuming that the signal collected by the i-th accelerometer deployed on the structure is formed of a part representing the structural response and an instrumentation noise term $\eta_i[t]$, as shown in Fig. 2, Eq. (5) can be rewritten as

$$x_i[t] = \sum_{m=1}^{\infty} \phi_{i,m} \ddot{q}_m[t] + \eta_i[t] \tag{21}$$

where $x_i[t]$ is the acceleration collected by the i-th sensor and $\phi_{i,m}$ is the i-th element of the m-th mode shape. Assuming the noise term as white Gaussian, i.e., having an ideally flat spectrum, each modal contribution in the summation of Eq. (21) has a limited range in frequency where the structural response is higher than the instrumentation noise. Therefore, modal responses can be extracted using suitable bandpass filters with impulse responses $\bar{b}_m[\tau]$ centered at the natural frequencies of the systems ω_m and having a width equal to the frequency band that exceeds the noise threshold.

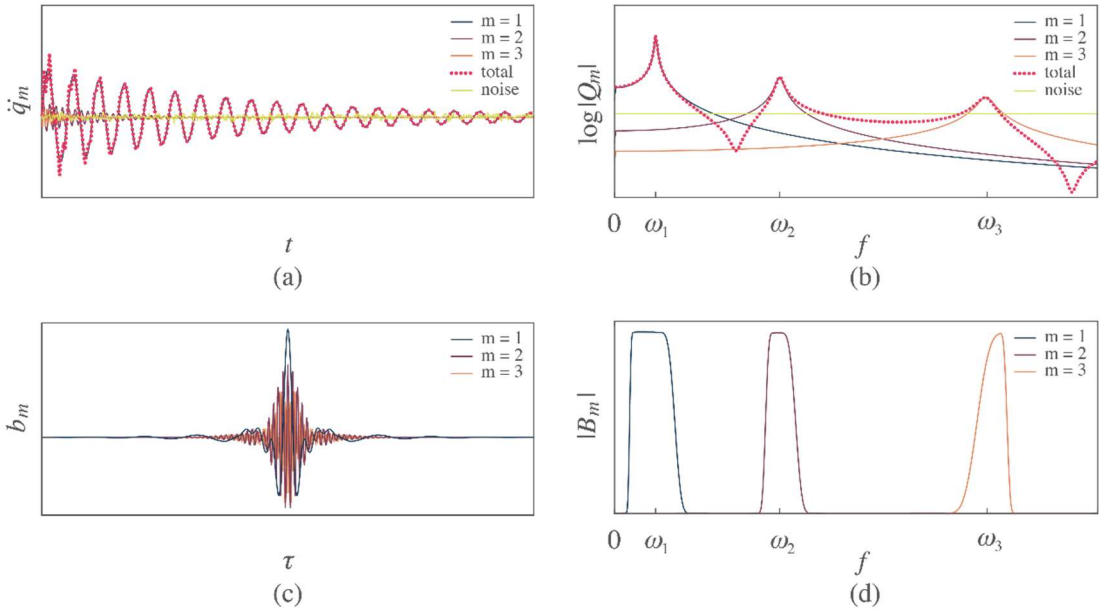

Fig. 2 – Modal components of the structural response in time (a) and frequency domain (b); bandpass filters in time (c) and frequency domain (d)

It has been recently shown how these filters can be simultaneously generated and applied to the collected data to extract modal contributions adaptively through the MAD [6]. The MAD is a two-dimensional representation of multivariate structural response, which highlights the presence of different modal contributions in frequency and time. It can thus be employed to identify and filter the modal responses automatically. Herein, the main concepts of the MAD are briefly reported; Interested readers may refer to reference [6] for a more exhaustive theoretical background. Then, a filter bank suitable for the extraction of modal contributions in civil infrastructures under moving loads is generated based on this technique. It is also shown how modal parameters, i.e., natural frequencies and mode shapes, can be identified from decoupled modal responses.

2.2.1 Modal assurance distribution

Applying a narrow bandpass filter $b_m[\tau]$ with cutoff frequencies $\omega_m - \epsilon$ and $\omega_m + \epsilon$ to the structural response $x_i[t]$, where ϵ is a sufficiently small number and ω_m is a resonant frequency of the structure, the filtered structural response can be written considering a single term of the summation of Eq. (21) as

$$y_{i,m}[t] \cong \phi_{i,m}(\ddot{q}_m * b_m)[t] + \eta_{i,m}[t] \tag{22}$$

where $\eta_{i,m}[t]$ is a filtered noise component. As shown in Fig. 2(b), the significant content of $\ddot{q}_m[t]$ is indeed generally concentrated into a narrow frequency range. Neglecting the noise component and calculating $y_{i,m}[t]$ for all the instrumented locations, an estimate of the i-th element of the instantaneous m-th mode shape $\boldsymbol{\phi}_m[t]$ of the structure can be obtained as

$$\phi_{i,m}[t] \cong \frac{x_{i,m}[t]}{x_{r,m}[t]} \tag{23}$$

where r denotes a reference location considered for normalization. It should also be noted that bandpass filters with slightly different cutoff frequencies, say ω_m and $\omega_m + 2\epsilon$, provide quite accurate estimates of the m-th mode shape if ϵ is small enough.

On the other hand, using a filter $b_k[\tau]$ centered at a frequency ω_k far from the resonant frequencies of the structure, the contribution of $\eta_{i,m}[t]$ is likely to prevail over the structural response in Eq. (22). Moreover, considering another filter $b_{k+1}[\tau]$ with different frequency range, far from ω_m, the filtered component is not correlated with the previous one due to the properties of white Gaussian noise.
In general, the result of Eq. (23) evaluated using a generic bandpass filter $b_k[\tau]$ can be interpreted as an element of the instantaneous operating deflection shape (ODS) of the structure evaluated at the frequency ω_k. Herein, two different symbols will be used to indicate mode shapes (namely, $\boldsymbol{\phi}$) and ODSs (namely, $\boldsymbol{\varphi}$). Also, the index m indicates a vibration mode of the structure, while k indicates a generic frequency band. It should be noted that the ODS $\boldsymbol{\varphi}_k$ becomes an estimate of the m-th mode shape $\boldsymbol{\phi}_m$ only if ω_k is close enough to the natural frequency of the system ω_m. Moreover, using a filter bank formed of narrow bandpass filters with consecutive cutoff frequencies, the ODS $\boldsymbol{\varphi}_k[t]$ will be persistently similar to $\boldsymbol{\varphi}_{k+1}[t]$ only if the k-th band is close to a resonant frequency of the system. Here, the term "persistently" is intended in time, since random similarities between two consecutive ODSs may also be generated by instantaneously similar noise components. The MAD aims to quantify and localize such similarities on a time-frequency plane. In particular, the elements of the MAD matrix $\mathbf{M}$ are defined as

$$M_{k,t} = \frac{\left|\boldsymbol{\varphi}_k^{\mathrm{T}}[t]\boldsymbol{\varphi}_{k+1}[t]\right|^2}{\left(\boldsymbol{\varphi}_k^{\mathrm{T}}[t]\boldsymbol{\varphi}_k[t]\right)\left(\boldsymbol{\varphi}_{k+1}^{\mathrm{T}}[t]\boldsymbol{\varphi}_{k+1}[t]\right)} \tag{24}$$

and are in the range between 0 and 1, where values close to 1 denote the presence of similar ODS in consecutive frequency bands (i.e., k and $k+1$), while values close to 0 indicate the presence of orthogonal consecutive ODSs. Therefore, the high-valued regions in the time-frequency (t-k) plane indicate frequency bands close to the natural frequencies of the system. Beta-distributed noise populates the remaining parts of the plane.
The bandpass filters employed in the literature to generate the MAD are obtained through the wavelet transform. In [6], critically-sampled transform coefficients were generated using wavelet packet filter banks to reduce the weight of the distribution. Conversely, in [7], an overcomplete wavelet expansion was employed to build filters able to extract oversampled representations of the non-linear normal modes of the structure during strong short-term events. In both the approaches, Parseval's theorem enabled the assumption of $\boldsymbol{\varphi}_k[t]$ as ODSs of the systems.

2.2.2 Extraction of decoupled modal contributions
In this study, wavelet analysis filters of the Fejér-Korovkin family are employed to calculate the MAD, implementing a stationary wavelet packet transform (SWPT) without downsampling. However, the filters of any linear time-frequency decomposition (e.g., Fourier complex exponentials or other wavelet functions) can be employed for this purpose.
Considering $g_{a,k}[\tau]$ the impulse response of the equivalent SWPT analysis filter associated with the k-th component, the ODSs of the structure can be calculated by filtering the collected acceleration $x_i[t]$:

$$\varphi_{i,k}[t] = \left(x_i * g_{a,k}\right)[\tau] \tag{25}$$

In Eq. (25), $\varphi_{i,k}[t]$ are the wavelet components, with $k = 1, \dots, 2^n$, resulting from an SWPT of level n. The vector $\boldsymbol{\varphi}_k[t]$ that includes the elements $\varphi_{i,k}[t]$ calculated at all the instrumented locations represents an instantaneous ODS of the structure at the k-th frequency band and can be employed in Eq. (24) to calculate the MAD.
The regions of the time-frequency plane containing relevant information on the structure can be selected by posing a threshold on the MAD values. Specifically, using a user-defined threshold θ, only the elements $M_{k,t} \geq \theta$ will be considered for the identification of decoupled modal contributions. In [6], different criteria for selecting the optimal θ threshold are discussed, showing its dependence on the number of

sensors. The elements $\boldsymbol{\varphi}_k[t]$ for which the condition $M_{k,t} \geq \theta$ is satisfied can be partitioned into different sets using a clustering algorithm. In [6], image segmentation of high-valued regions of the MAD and the modal assurance criterion (MAC) were employed to define the modal clusters. Conversely, in [7], the k-means algorithm was used, together with self-organizing maps to determine the number of clusters. In this study, the density-based spatial clustering of applications with noise (DBSCAN) algorithm is employed for clustering, which does not require a preliminary knowledge of the number of clusters [35].
At the end of the clustering procedure, each cluster will correspond to a different mode of the structure. Considering the m-th cluster, the related 'clustered' filter which can be used to extract the m-th modal contribution at all the instrumented locations at the t-th instant can be calculated as

$$\bar{b}_m^{(t)}[\tau] = \sum_{k=k_1}^{k_2} \left(g_{a,k} * g_{s,k}\right)[\tau] \tag{26}$$

where the $k = k_1, \dots, k_2$ is the index of the ODSs contained in the m-th cluster. The modal component $x_{i,m}[t]$ can be extracted using the clustered filter as follows:

$$x_{i,m}[t] = \left(x_i * \bar{b}_m^{(t)}\right)[t] \tag{27}$$

It should be noted that the cutoff frequencies of $\bar{b}_m^{(t)}$ vary over time according to the result of the clustering process. This allows the filter bank to be adaptive and follow changes in the structural behavior due to varying environmental and operational conditions.

2.2.3 Consideration on multiple moving loads

Although the application of the MAD-based decomposition algorithm in the case of a single moving load is similar to the case of impulsive load or broadband noise excitation, the presence of multiple loads theoretically affects the outcome of the procedure. In particular, considering a vehicle having two wheel axles, the frequencies close to $\bar{f}_r$ are suppressed in the structural response due to the particular spectrum of the load function shown in Fig. 1(d). Nevertheless, in real applications, vibration transmitted by the adjacent spans – due to the passage of other vehicles – and other loads, such as wind, will form a more complex loading function, which can be represented in the form:

$$p(z,t) = v(z,t) + P[\delta(x - vt) + \delta(x - w - vt)] \tag{28}$$

where $v(z,t)$ is an additional distributed noise function due to ambient and operational vibration. Considering the structure as a linear system, the structural response will include the effects of both moving loads and environmental phenomena. While the first are likely to prevail, the other effects produce contributions of the structural response that populate the spectral ranges close to $\bar{f}_r$. The similarity of the ODSs that generate high-valued regions in the MAD is intended in a vectorial sense (cosine similarity), i.e., ODSs which have similar ratios between their elements will generate MAD values close to 1, regardless of the amplitude of each specific element of $\boldsymbol{\varphi}_k[t]$. Therefore, the MAD does not depend directly on the amplitude of the signal components. For this reason, if the term $v(z,t)$ generates a structural response that exceeds the noise floor level of the accelerometers in all the frequency spectrum, the MAD will be robust to suppressed frequency bands due to multiple loads.

3. NOVEL STRATEGY FOR SHM OF CIVIL INFRASTRUCTURES

In Section 2.1, a method for estimating dense structural quasi-static features of a structure modeled as a simply supported beam using potentially a single sensor is shown. In particular, a lowpass filter is employed to extract the curvature influence line of the structure from acceleration data. Besides, in Section 2.2, the theoretical framework of the MAD is extended to the case of moving loads. It is shown that adaptive bandpass filters can be used to extract decoupled modal responses. The first features can provide valuable information about the location of structural anomalies and may give an idea of the damage entity. However, they are sensitive to noise and dynamic effects. On the other hand, modal parameters are only defined at the instrumented locations but are generally more robust to noise. Thereby, a combination of the information obtained through the two aforementioned features may provide insights about the presence, approximate location, and entity of structural damage. In the following, a novel strategy for SHM of civil infrastructures is presented based on these concepts. Specifically, a filter bank that includes the filters able to extract both quasi-static and dynamic features is first presented. Then, an approach for damage identification is proposed based on the identified features.

3.1 Structural identification

Considering a set of column vectors $\mathbf{b}_j^{(t)}$ containing the coefficients of the impulse responses $\bar{b}_j^{(t)}[\tau]$ with $\tau = 1, \dots, N$, where N is the filter length, a filter bank matrix at the t-th time instant can be represented as follows:

$$\mathbf{B}_t = \left[\mathbf{b}_0, \mathbf{b}_1^{(t)}, \dots, \mathbf{b}_p^{(t)}\right] \tag{29}$$

Here, the term $\mathbf{b}_0$ contains the coefficients of the lowpass filter $\bar{b}_0[\tau]$ used in Section 2.1 to extract the quasi-static structural features. In this study, it is assumed that $\mathbf{b}_0$ does not depend on the time instant, i.e., the lowpass filter does not evolve over time, and therefore the apex (t) is dropped. On the other hand, the terms $\mathbf{b}_j^{(t)}$ with $j = 1, \dots, p$ indicate the adaptive time-dependent bandpass filters.
Considering a matrix $\mathbf{X}_t$ with the form

$$\mathbf{X}_t = \left[\mathbf{x}_{t,1}, \mathbf{x}_{t,2}, \dots, \mathbf{x}_{t,r}\right] \tag{30}$$

where $\mathbf{x}_{t,i}$ are column vectors containing the samples of the acceleration signal $x_i[t]$ in the interval $[t - N/2, t + N/2]$, a set of decomposed signals can be computed as:

$$\mathbf{Y}_t = \mathbf{X}_t^{\mathrm{T}}\mathbf{B} = \begin{bmatrix} y_{1,0}[t] & y_{1,1}[t] & \cdots & y_{1,p}[t] \\ y_{2,0}[t] & y_{2,1}[t] & \cdots & y_{2,p}[t] \\ \vdots & \vdots & \ddots & \vdots \\ y_{r,0}[t] & y_{r,1}[t] & \cdots & y_{r,p}[t] \end{bmatrix} \tag{31}$$

It should be noted that the elements $y_{i,0}[t]$, upon changing the variable in $z = vt$, represent the estimates of curvature at the i-th location, when the load is applied in z. Conversely, due to the Maxwell-Betti reciprocal work theorem, $y_{i,0}[t]$ can also be interpreted as the structural curvature in z generated by a static load applied at the i-th instrumented location. On the other hand, the terms $y_{i,m}[t]$ with $m = 1, \dots, p$ are the t-th samples of the m-th modal responses collected at the i-th location.
When moving loads enter and leave the monitored bridge span, a peak in acceleration is typically registered due to the dynamic effect of the load passing on the bridge joint. These peaks can be used in an automated procedure to trigger the calculation of quasi-static and dynamic structural features. The parameters

identified in these time intervals can thus be averaged by considering different passing vehicles to improve the robustness of the estimate. In particular, the curvature influence line in position ζl (which is the i-th instrumented location) can be computed as

$$h^{(\zeta)}[z]\big|_{z=vt} = y_{i,0}[t] \tag{32}$$

with $t = 0$ the instant when the load enters the bridge span and $t = l/v$ the instant when the load leaves the bridge span. An average influence line $\bar{h}^{(\zeta)}[z]$ can be computed upon normalization (e.g., to the maximum value in the considered interval) to remove the dependence on the vehicle weight. Considering baseline and inspection estimates of the average influence lines identified in two different time instants, the (spatial) point-by-point difference between them can be employed as a dense feature for damage identification. It should be noted that the spatial resolution of this feature depends only on the sampling frequency of $y_{i,0}[t]$. A schematic workflow of the procedure proposed is illustrated in Fig. 3: Upon collecting the signals and building the filter banks through the MAD – which can be updated at given time intervals (1), analysis windows are selected as the intervals between the entering and leaving of a vehicle in the bridge span (2); The acceleration signals are then filtered (3) and normalized (4) to obtain sparse estimates of the modal parameters at the instrumented locations and dense curvature influence lines. Modal parameters, intended as frequencies and amplitudes of $y_{r,p}[t]$, can be easily extracted either in the time (e.g., using the Hilbert transform [6] or non-linear energy operators [5]) or frequency domain (e.g., peak picking). Both dense and sparse identified parameters can then be employed for damage identification.

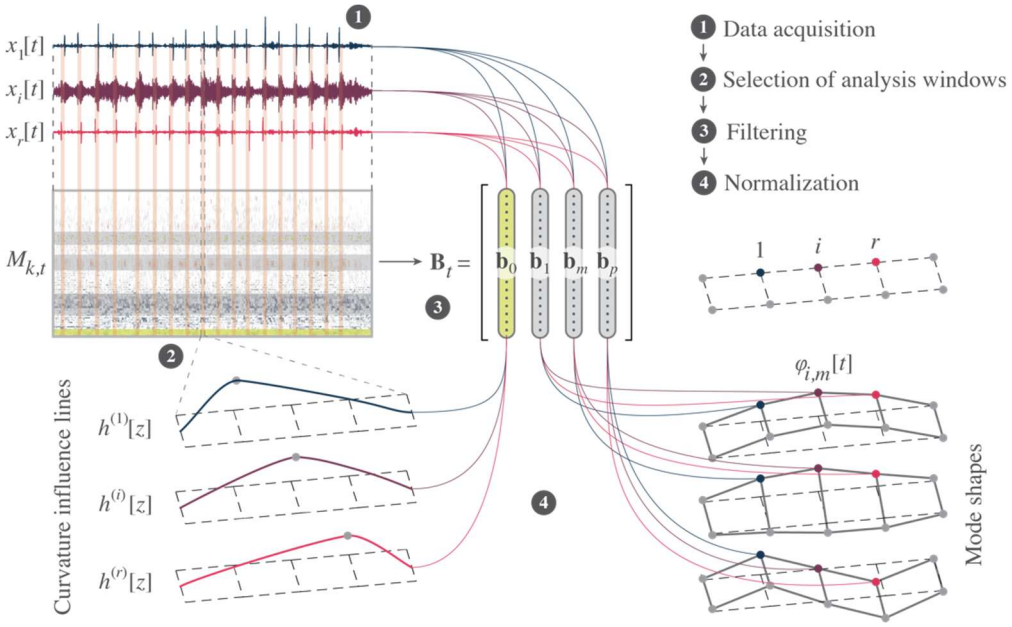

Fig. 3 – Workflow of the procedure proposed for feature extraction

It should be noted that an alternative sparse estimate of the structural curvature under a force applied at the i-th instrumented location can be obtained using the modal parameters identified from decoupled modal contributions. An estimate of the flexibility matrix of the structure is indeed

$$\mathbf{F} \cong \sum_{m=1}^{p} \frac{1}{\omega_m^2} \boldsymbol{\phi}_m \boldsymbol{\phi}_m^{\mathrm{T}} \tag{33}$$

where p is the number of identified modes and ω_m is the m-th natural circular frequency. Considering a load vector $\mathbf{u} = [0, \dots, 1, \dots, 0]^{\mathrm{T}} \in \mathbb{Z}^{r\times 1}$ with a single nonzero element at the i-th location, the deflection shape of the structure reads

$$\mathbf{u} = \mathbf{F}\mathbf{p} \tag{34}$$

The curvature can then be calculated using a finite difference method, e.g., the central difference. Average curvature values considering multiple vehicle passages can be employed to generate baseline and inspection features, which may be compared for damage identification.

3.2 Damage identification

In the common practice, structural damage is assessed by comparing two states of the monitored system, namely, a baseline (here addressed as "undamaged") condition and an inspection (possibly damaged) condition. In this study, the structural curvature is used as a DSF. In particular, we assume that an increment in curvature is representative of damage, modeled as a local stiffness loss. This way, the difference in the curvature estimate, obtained either from influence lines or modal parameters, calculated between the inspection and the baseline condition is assumed here as a damage index. Therefore, prominent peaks in the function of the damage index indicate damaged areas.

The magnitude of the difference of curvature (here called "difference function" for simplicity), under certain assumptions, can also be representative of the damage entity. In the following, these assumptions and the method proposed to quantify structural damage using the identified influence lines are described in detail.

As aforementioned, for a simply supported beam, according to the Maxwell-Betti theorem, the influence line calculated in a given location using a moving load has the same profile of the beam deflection shape when it is subjected to a load applied at the instrumented location. In isostatic structures, the bending moment distribution $M[z]$ due to an unknown concentrated load applied at a certain location $z = \zeta l$ do not depend on the structural stiffness $EI[z]$ and has a triangular shape with a maximum $M_\zeta = M[\zeta l]$. In this case, the difference between the normalized curvatures $\bar{h}_u^{(\zeta)}[z]$ and $\bar{h}_d^{(\zeta)}[z]$ identified in a baseline and inspection time intervals, respectively, can be written as

$$\Delta\chi(z) = \bar{h}_d^{(\zeta)}[z] - \bar{h}_u^{(\zeta)}[z] = \frac{M[z]}{C_d EI_d[z]} - \frac{M[z]}{C_u EI_u[z]} \tag{35}$$

where the normalization factors C_u and C_d are

$$C_u = \max\left(\frac{M[z]}{EI_u[z]}\right);\ C_d = \max\left(\frac{M[z]}{EI_d[z]}\right) \tag{36}$$

Let $EI_u[z] = EI_u$ be constant with z in the undamaged condition and consider the damage as a localized stiffness reduction at the location $\bar{z}$ with the following constraint on the damage entity:

$$EI_d[\bar{z}] \geq \frac{M[\bar{z}]}{M_\zeta} EI_u \tag{37}$$

This condition is assumed to have the normalization factors both equal to

$$C_u = C_d = \frac{M_\zeta}{EI_u} \tag{38}$$

In this case, Eq. (35) in the damaged location becomes

$$\Delta\chi[\bar{z}] = \frac{M[\bar{z}]}{M_\zeta}\left(\frac{EI_u}{EI_d[\bar{z}]} - 1\right) \tag{39}$$

The local stiffness of the damaged beam can thus be identified as:

$$EI_d[\bar{z}] = \beta[\bar{z}]EI_u \tag{40}$$

with

$$\beta[\bar{z}] = \left(\frac{M_\zeta}{M[\bar{z}]}\,\Delta\chi[\bar{z}] + 1\right)^{-1} \tag{41}$$

It should be noted that the ratio $M_\zeta/M[\bar{z}]$ can be easily determined upon localizing the damage (i.e., localizing a peak in the difference function) and does not depend on the load magnitude but only on its position (i.e., the instrumented location). Moreover, due to the assumption of Eq. (37), a reliable value of β can be effectively determined only far from the instrumented location. On the other hand, close to the instrumented location, a local maximum in the curvature function still describes the damage location, but its amplitude is not representative of the damage entity.
It should also be observed that, for a given cutoff frequency f_l of the lowpass filter used to identify the influence line, the accuracy of β depends on the speed of the vehicle v and the spatial extension of the damage. Specifically, the frequency of the filtered signal should be high enough to describe the localized irregularity of the curvature properly, i.e., the period of the filtered signal should be at most half the time it takes for the vehicle to overcome the damaged part. In other words, the minimum spatial extension of the damage to properly identify its entity is:

$$D_{min} = \frac{v}{2f_l} \tag{42}$$

4. APPLICATIONS

4.1 Structural identification: Italian A24 motorway

In this section, the data collected by the University of L'Aquila during an experimental campaign conducted between February and June 2019 on the viaducts of the A24 motorway will be used to test the proposed methods. The Italian A24 motorway connects Rome to the Adriatic Sea and has a considerable number of viaducts, given the complex orography of the territory. Many viaducts consist of single-span post-tensioned prestressed beams in a simply-supported isostatic configuration (Fig. 4). The trapezoidal cross-section, shown in Fig. 5, is 2.3m high and has two 3.85m-wide cantilevered wings. The bridge spans are supported by pairs of piers with a hollow cross-section placed at a center distance of about 40m.

(a) (b)

Fig. 4 – Detail of the supports (a) and side view of an A24 viaduct (b) [9]

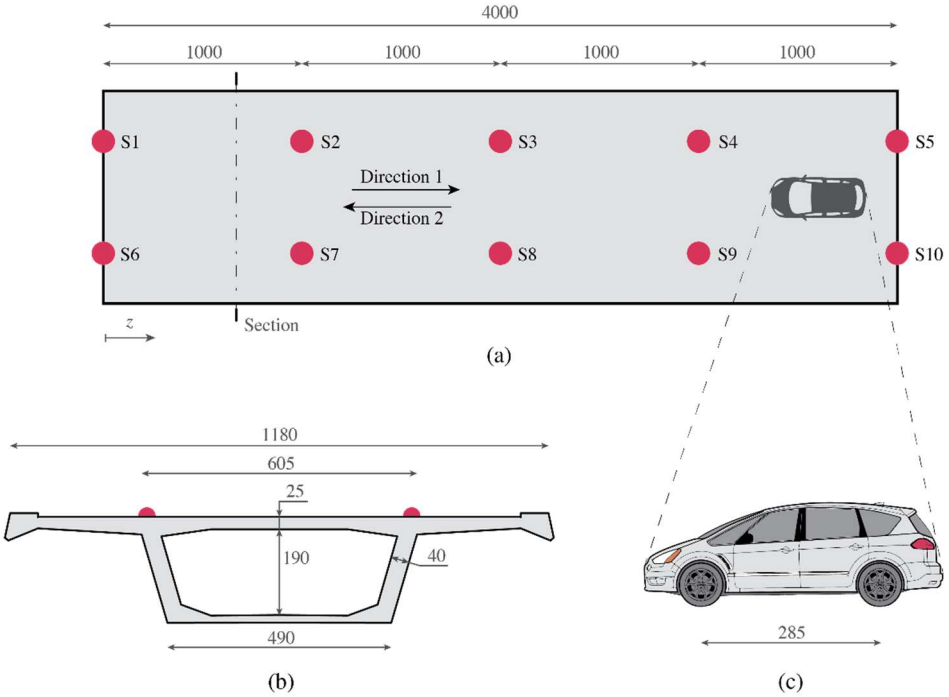

Fig. 5 – Plan (a) and section (b) views of the bridge spans, adapted from [9]*, and car scheme (c); dimensions in cm*

Ten biaxial force-balance accelerometers (FBAs) were used to record the deck response to traffic excitation, deployed as shown in Fig. 5. The accelerometers were organized in two measurement chains, each guided by the main recording unit connected to a Wi-Fi access point and synchronized by GPS. The data was originally sampled at a frequency of 200 Hz, and an anti-aliasing filter with a cutoff frequency of 40 Hz was used.

In this paper, three viaducts are studied, namely, Cerchiara, Temperino, and Biselli. Acceleration time histories of 1500 s collected in the vertical direction and downsampled at 50 Hz are employed for structural identification. In these time intervals, a car with a mass of 1750 kg and wheel axles distant 2.85 m, as shown in Fig. 5(c), excited the bridge by moving back and forth (in this paper addressed as Direction 1 and Direction 2) multiple times, at a speed of between 30 and 60 km/h.

The accelerometers S1, S5, S6, and S10 are located near the expansion joints. The recordings of these devices are used to select the signal intervals recorded during the passage of the car, as shown in Fig. 6, where the acceleration signals collected on the Cerchiara viaduct are shown. In particular, considering the speed and the geometry of the car, two close acceleration peaks (i.e., distant in time between 0.2-0.4 s, generating by the wheels passing on the expansion joints) are used as a triggering sequence to identify the passing car. Specifically, a triggering sequence in sensor S1 followed by a triggering sequence in S5 within

6 s indicates a car driving in Direction 1. Conversely, a triggering sequence in sensor S5 followed by a triggering sequence in S1 within the same time interval indicates a car driving in Direction 2. In this paper, individual moving cars have been considered. The identified intervals will be used in the evaluation of quasi-static and dynamic structural features.

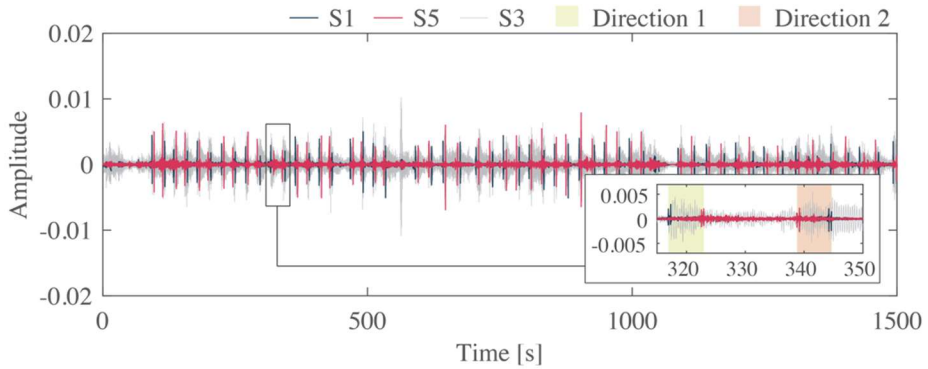

Fig. 6 – Collected acceleration and identification of passing vehicles (Cerchiara viaduct)

In order to build a filter bank capable of extracting the modal responses of the structure, the MAD was applied to the multivariate signal consisting of all the 10 recording channels. The SWPT was used to obtain the preliminary signal decomposition, employing the Fejér-Korovkin 22 wavelet function in the procedure outlined in Section 2.2.2. As shown in the same section, a DBSCAN procedure was then applied to the relevant ODSs, identifying four different vibration modes (for all the three viaducts), represented in Fig. 7 on a time-frequency plane. In the application of the DBSCAN algorithm, a neighborhood search radius of 0.1 was used, employing the Euclidean distance as a distance metric. In Fig. 7, the $M_{k,t}$ elements obtained for the Cerchiara viaduct are represented in two dimensions, where t is the time index and k indicates the frequency subband (rescaled between 0 and 25 Hz, i.e., the Nyquist frequency of the downsampled signal employed in this study). White regions in Fig. 7 indicate MAD values close to 0, while the elements that exceed the θ threshold (here selected as 0.5) are partitioned into four clusters indicated by different colors. A zoom view is reported in the upper-right part of the figure to better show the components related to the higher modes, which are generally more difficult to identify.
The equivalent bandpass filters which can be used to extract the identified modes are calculated as shown in Eq. (26). It should be noted that, in this study, the time dependence of the cutoff frequencies is neglected since the structural behavior in the short term does not present varying modal features. In the left-lower part of Fig. 7, the four frequency bands analyzed to extract the modal contributions are highlighted.

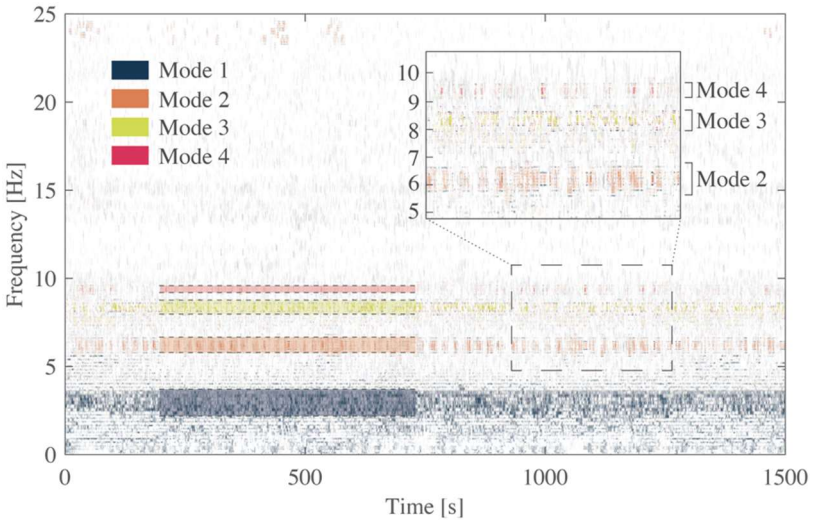

Fig. 7 – Modal assurance distribution and identification of vibration modes (Cerchiara viaduct)

For each time interval identified during the car passage, here addressed as "sample interval" or simply "sample", the modal parameters are estimated by applying the Hilbert transform to the decoupled modal contributions. The mean of the instantaneous frequencies calculated through the Hilbert transform is reported in Fig. 8 for each sample. It is possible to observe that slight variations may manifest in identified frequencies. The robustness of the identification can be improved by considering average estimates computed over a large set of samples. The average values of modal frequencies are reported in Fig. 9, together with the average amplitudes of the mode shapes. It should be noted that, due to the comparable geometry of the viaducts, the modal parameters of the different case studies are similar. Moreover, the mode shapes are in good agreement with the estimates obtained through the frequency domain decomposition (FDD) [36], a traditional modal identification algorithm applied in this study to the entire set of signals with a duration of 1500 s.

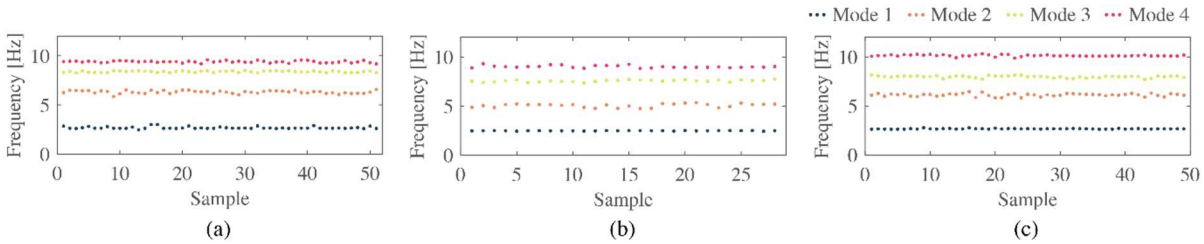

Fig. 8 – Identified natural frequencies for each acceleration sample: Cerchiara (a), Temperino (b), and Biselli (c).

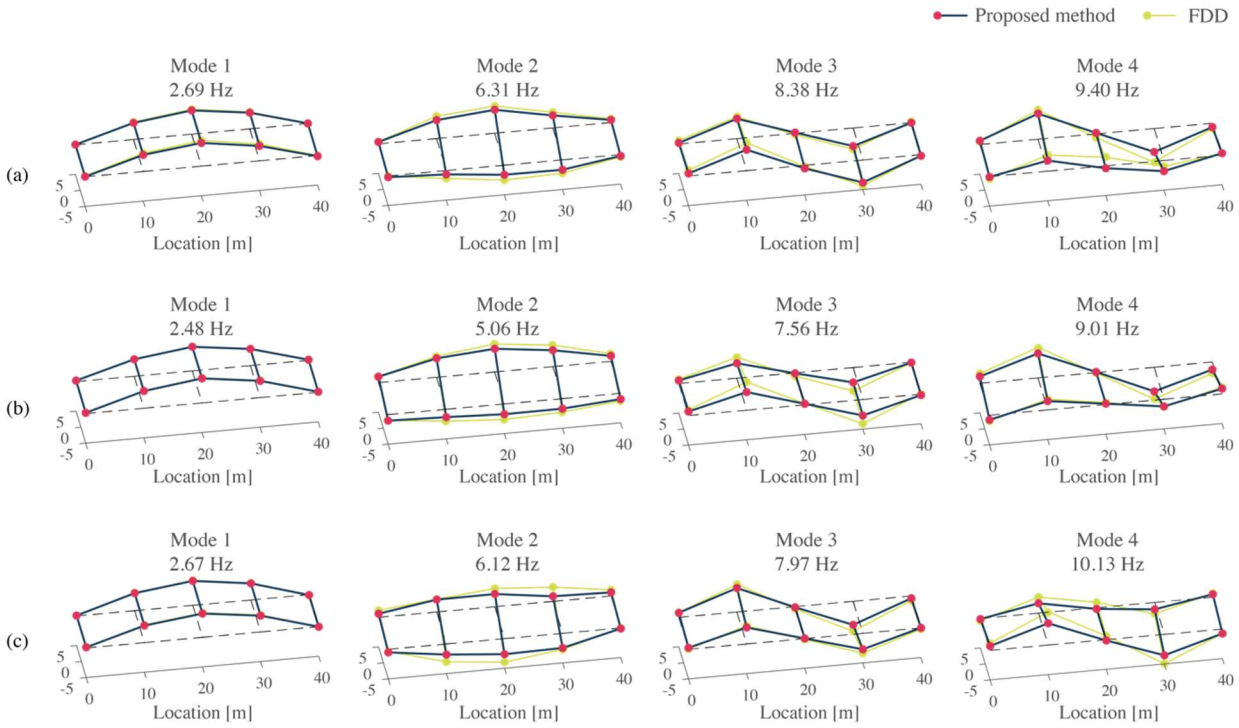

Fig. 9 – Identified average mode shapes: Cerchiara (a), Temperino (b), and Biselli (c).

In this case study, the elements of the lowpass filter $\mathbf{b}_0$ used for the extraction of the quasi-static features has been selected considering a clustered filter consisting of the first two wavelet filters, i.e.,

$$b_0[\tau] = \left(g_{a,1} * g_{s,1}\right)[\tau] + \left(g_{a,2} * g_{s,2}\right)[\tau] \tag{43}$$

In Fig. 10, the lowpass filtered signal $y_{i,0}[t]$ obtained for the Cerchiara viaduct is reported for sensors S2, S3, and S4. The highlighted intervals are the identified samples related to passing cars. In the zoom view, it is possible to observe that the maxima of the filtered signals are consistent with the locations where they are collected. Specifically, the signal related to S2 has a maximum in the left part of the sample interval when the car moves in Direction 1, while the signal collected in S4 has a maximum in the right part of the identified interval. Conversely, the order of the peaks is exchanged in the interval related to Direction 2. Moreover, the signal of sensor S3 has a maximum between the other two in both configurations.

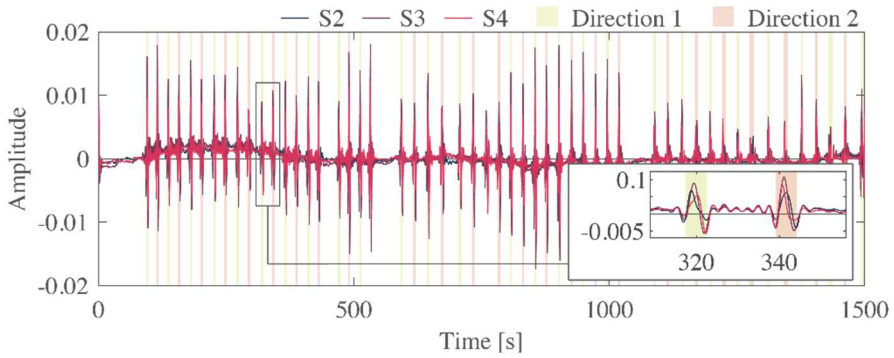

Fig. 10 – Low-frequency filtered acceleration component and identification of influence lines (Cerchiara viaduct)

Different estimates of the curvature influence lines are extracted from the sample intervals and the estimates related to Direction 2 are switched before changing the time variable t into the spatial variable $z = vt$. Then, the extracted curves have been interpolated to have the same number of points (in this case, 100 points), representing a regular set of equally-spaced locations. In Fig. 11, all the estimates of the influence line are shown in gray for each case study and sensor location. In particular, each gray line represents the mean between the influence lines calculated in a given sample interval by the two sensors at the opposite sides of the deck (indicated in the lower-right corner of each plot). The average of the identified influence lines is also reported in magenta and compared with the curvature of the structural deflection calculated using the flexibility matrix (only at the three instrumented locations) as shown in Eq. (34), represented in blue. The flexibility-based curvature has been evaluated using the set of identified modal parameters, as indicated in Eq. (33), and the results shown in Fig. 11 are obtained as the mean of the lines evaluated at the two sides of the deck. In general, the curvature (or bending moment) influence line of a simply-supported beam should have two linear segments, with a maximum in the point where the influence line is evaluated (in this case, the instrumented location, highlighted by a vertical dashed line in Fig. 11). However, due to the lowpass filter applied to the acceleration time history in the proposed method, the higher frequency components that contribute to sharpening the influence line are dropped. Therefore, the influence line results smoother than the theoretical result. It should also be noted that only three points of curvature can be calculated using the flexibility-based method using the sensor layout of this application due to the limitations of the central difference method. The results obtained through the flexibility-based procedure are slightly different from the theoretical result, but they are in good agreement with the dense feature obtained through the proposed method. Despite the differences between the estimated values and the theoretical shape of the influence line, the results shown can be effectively used to localize structural anomalies in an SHM procedure. This aspect is shown in the numerical case study presented in the next section of this paper.

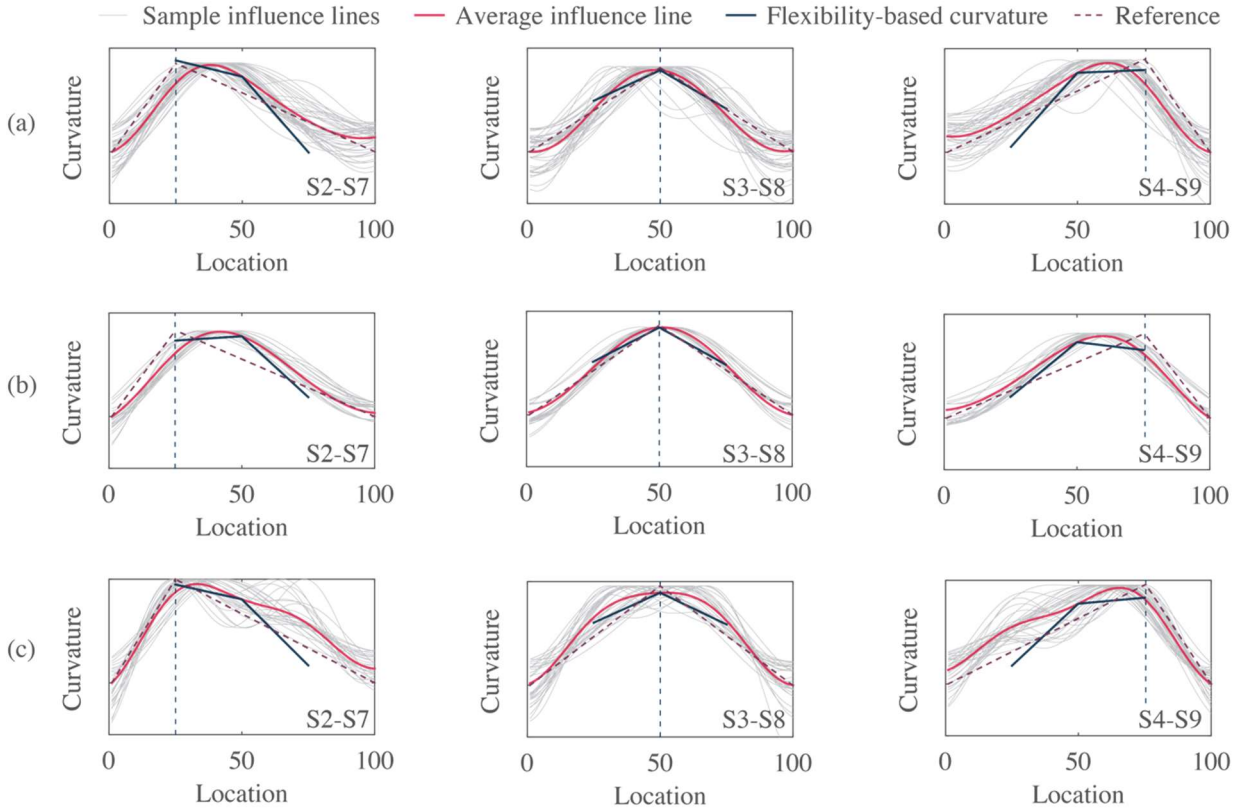

Fig. 11 – Identified curvature influence lines: Cerchiara (a), Temperino (b), and Biselli (c).

4.2 Damage identification: Numerical benchmark

The second case study analyzed in this paper is a numerical model of a simply-supported beam with structural characteristics similar to the viaducts analyzed in the previous section. Specifically, the length of the beam is 40 m and the cross-section is modeled as shown in Fig. 5(b), with an overall flexural stiffness $EI = 105.96 \cdot 10^6$ kNm^2. Modal damping of 5% has been assumed for all the vibration modes. Three uniaxial accelerometers have been simulated, collecting the acceleration in the vertical direction at the locations indicated in Fig. 12. A single row of sensors is used in this case study since the beam has been modeled as a unidimensional structure.

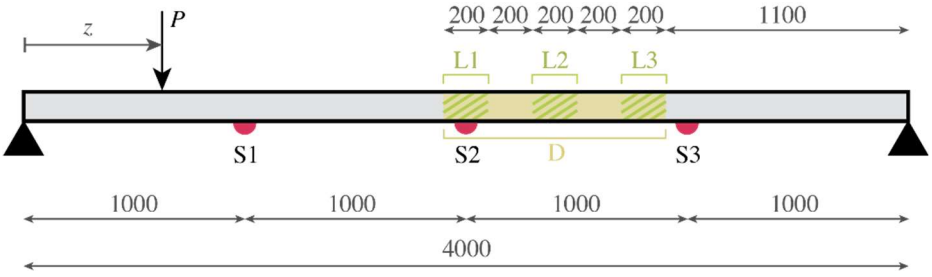

Fig. 12 – Scheme of the numerical benchmark; dimensions in cm.

In order to simulate the application of the damage identification procedure proposed in Section 3, four damage locations have been considered, resulting in the seven damage conditions summarized in Tab. 1. Specifically, individual or multiple localized damages (modeling the impacts generated by vehicles underneath the bridge or cracked regions) are simulated in the segments L1, L2, and L3. On the other hand, location D simulates a diffuse stiffness reduction (e.g., due to spalling), and is used to generate three damage conditions of different entity. In this case study, the moving load is modeled as a single force P, passing over the structure (from left to right, as shown in Fig. 12) with a constant speed.

Tab. 1 – Description of the damage conditions

Damage condition	Description
DC1	Flexural stiffness reduction of 30% in L1
DC2	Flexural stiffness reduction of 30% in L2
DC3	Flexural stiffness reduction of 30% in L3
DC4	Flexural stiffness reduction of 5% in D
DC5	Flexural stiffness reduction of 10% in D
DC6	Flexural stiffness reduction of 15% in D
DC7	Flexural stiffness reduction of 10% in L1 and 30 % in L3

In a first analysis, the influence lines have been determined by processing the clean acceleration signal, sampled at 100 Hz, collected in a single interval representing the passage of a moving load on the beam. Specifically, Fig. 13 shows the curvature influence lines (normalized to the maximum value) obtained through a lowpass filter consisting of the first two components of a WPT of level 7 (with a resulting cutoff frequency of 0.78 Hz) generated using the Fejér-Korovkin 8 function. The results obtained for each sensing location (indicated in the lower-right corner of each plot) and damage condition are plotted in solid lines, while the differences between the normalized influence lines calculated in the undamaged and each damaged scenario are reported as dotted lines. In this study, different vehicle speeds have been considered. In particular, Fig. 13(a) and (b) are obtained simulating the passage of a vehicle with a speed of 15 m/s. In this case, the location is discretized in 264 points. On the other hand, Fig.13(c) shows the results obtained using a speed of 3 m/s, and the location is discretized in 1332 points. It should be noted that each result is obtained considering only one sensor.

In the cases of localized damage, clear local maxima of the difference functions (highlighted by a circle) are close to the real damaged areas, independently of the vehicle speed. However, sharper peaks can be identified using the slow vehicle. In this situation, it is also possible to identify the presence of multiple damages (condition DC7). Similarly, high values in the difference function are always identified in the proximity of the diffuse damage, and, in the case of a slow vehicle, the damage index is less affected by dynamic effects, resulting in a more accurate damage localization.

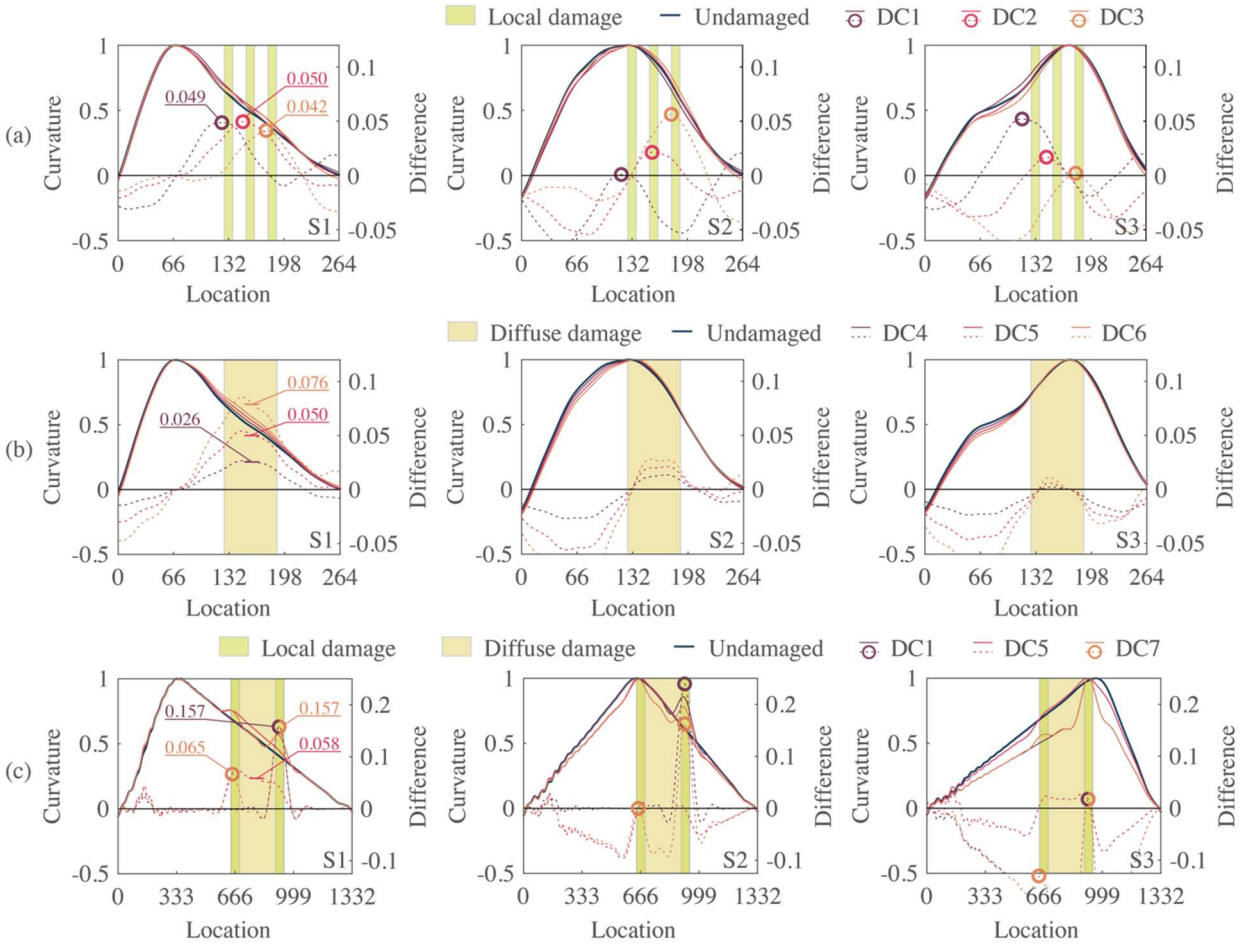

Fig. 13 – Influence lines identified in the numerical benchmark and difference functions for different damage entity and vehicle speed: (a) Local damage, 15 m/s; (b) Diffuse damage, 15 m/s; (c) Mixed damage, 3 m/s.

Upon identifying the location of the damaged areas, the stiffness loss can be quantified using Eq. (41). The results of damage quantification using the values identified by sensor S1 (explicitly written in Fig. 13) are reported in Fig. 14 in the form $(1-\beta)\cdot 100\%$. It should be noted that, according to Eq. (42), for a vehicle moving at 15 m/s, the smaller damage that can be correctly quantified has an extension D_{min} of 9.6 m (considering the lowpass frequency of 0.78 Hz corresponding to the first two wavelet components). Indeed, the identified values reported in Fig. 14(a) underestimate the damage entity since the damaged interval (2 m) is much lower than D_{min}. On the other hand, for the same vehicle speed, the entity values related to the diffuse damage reported in Fig. 14(b) are more accurate, especially for low damage levels. Finally, considering the vehicle speed as 3 m/s (for which D_{min} is 1.9 m), the damage entity can be correctly identified also for the localized damage conditions.

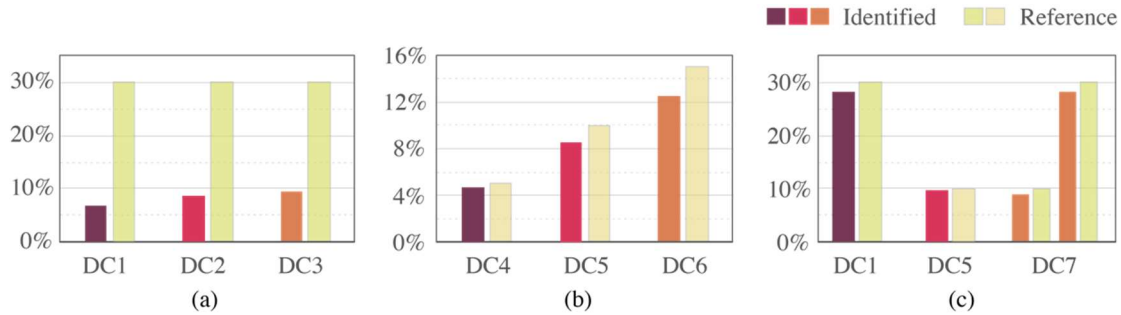

Fig. 14 – Identified damage entity for different vehicle speed: (a) Local damage, 15 m/s; (b) Diffuse damage, 15 m/s; (c) Mixed damage, 3 m/s.

While specific inspection vehicles traveling at 3 m/s can be used in a controlled environment (i.e., constant speed and exact path) with high-sensitivity accelerometers, faster vehicles are more representative of ordinary traffic conditions, where noise sources are generally non-negligible. Therefore, in further analysis, the recorded time histories have been polluted by introducing a considerable Gaussian white noise component with a standard deviation equal to the 50% of the standard deviation of the collected acceleration. The significant noise level represents different phenomena, including instrumentation noise, slightly non-constant vehicle velocity, and non-straight path. In this case, 100 sample intervals for the undamaged and each damage condition from DC1 to DC6 have been considered to calculate an average influence line from the normalized sample estimates, which is then used to compute the damage index (i.e., the difference function). The results of this analysis are reported in Fig. 15. Specifically, this figure shows the influence line obtained for each sample (thin lines), together with their average curves (thick lines), as well as the difference functions (dotted lines) for each sensor location (S1, S2, and S3) and damage conditions (from DC1 to DC6). In this case, the difference functions are corrupted by noise, and localizing damage becomes challenging. However, by combining the difference functions, i.e., by summing them for each spatial location, the damage localization can be improved, as shown in Fig. 16.

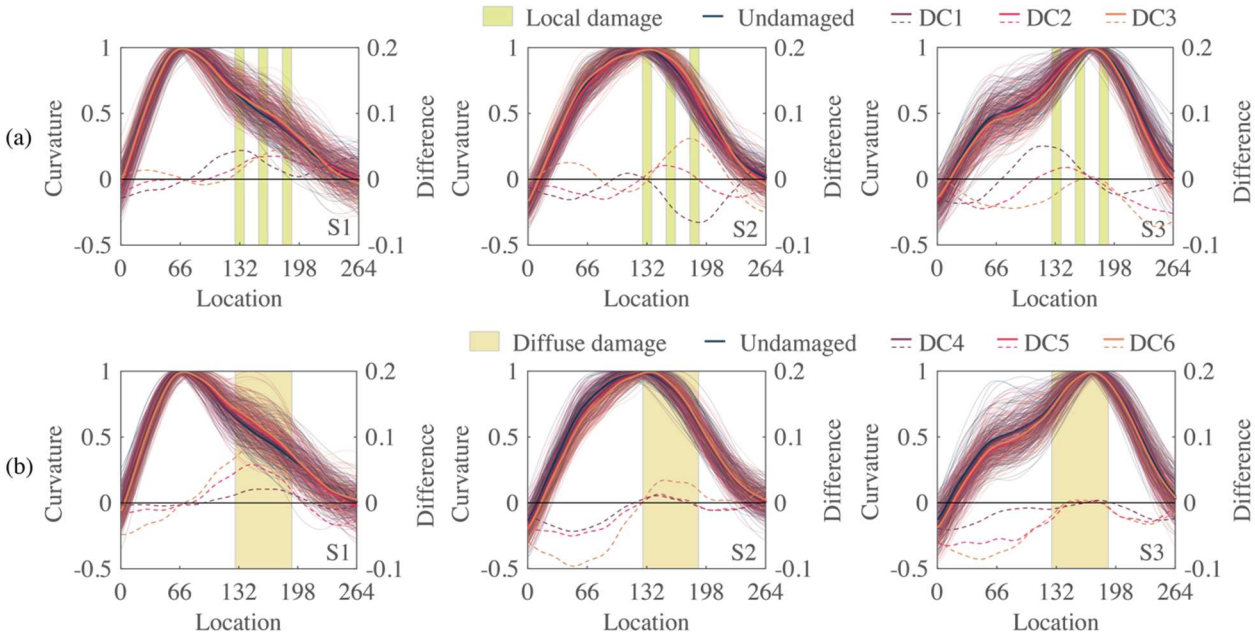

Fig. 15 – Influence lines identified in the simulated noisy environment (solid lines) and corresponding difference functions (dotted lined): (a) Local damage; (b) Diffuse damage.

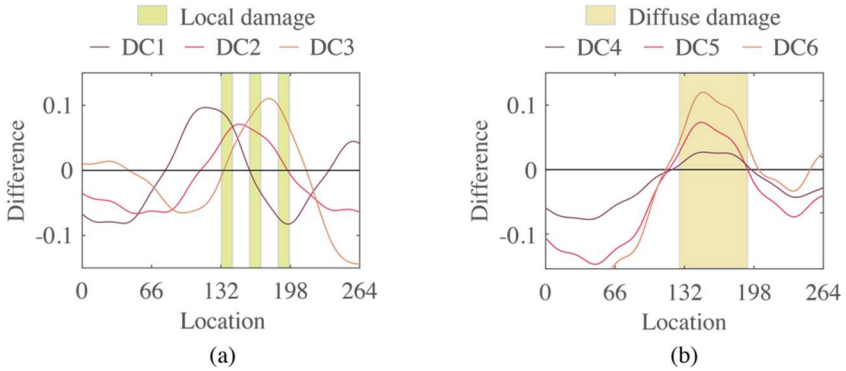

Fig. 16 – Cumulative difference function obtained in the simulated noisy environment: (a) Local damage; (b) Diffuse damage.

In a particularly noisy environment, peaks in the difference function can also be generated by dynamic effects. In such cases, although modal parameters cannot identify the exact location of damage, they can be employed to identify the damaged regions where the difference function peaks are likely related to actual damage. Fig. 17 shows the difference function obtained from the average curvature (computed on 100 noisy samples) obtained using the modal flexibility approach (as shown in Section 3.1). In particular, three structural deflections have been calculated considering a load vector **u** with the nonzero load element at location S1, S2, and S3, respectively, as indicated in the lower-right part of each plot. In all the cases, high values in the difference function are between sensors S2 and S3. This way, it is possible to understand that the local peaks in the difference functions obtained from the influence lines between locations 0 and 66 (Fig. 16(a)) are probably generated by dynamic effects and are not related to an actual stiffness loss.

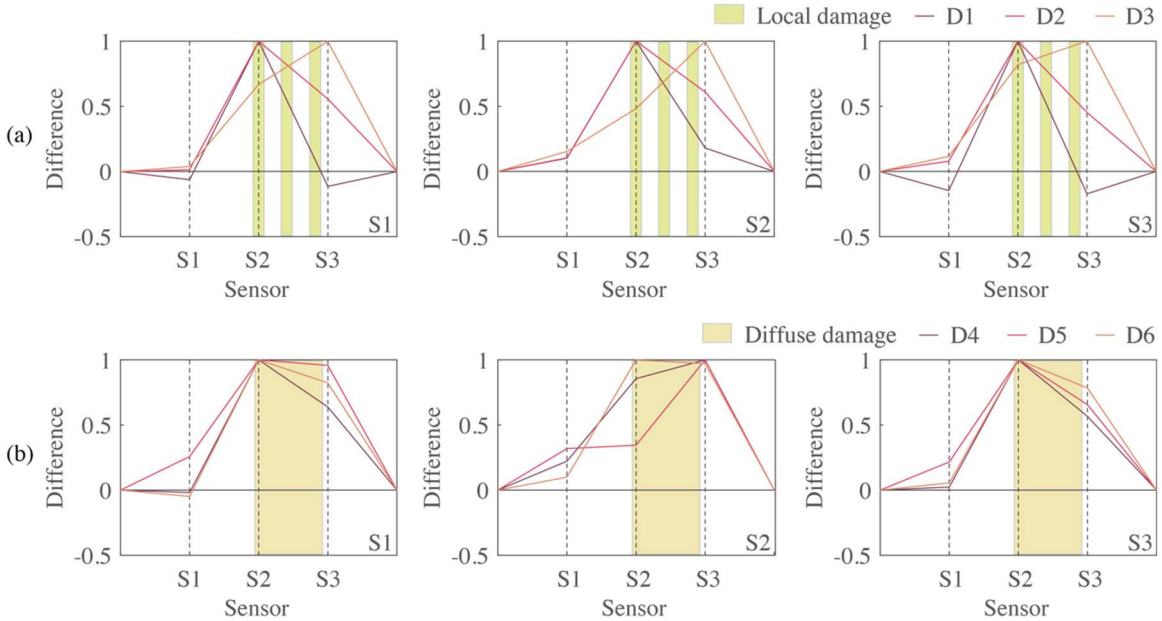

Fig. 17 – Normalized difference function obtained from modal parameters: (a) Local damage; (b) Diffuse damage.

The results obtained for damage quantification in the noisy environment using the influence lines identified at sensor S1are reported in Fig. 18. As expected, the local damage conditions are not correctly quantified. Moreover, the diffuse damage conditions show results less accurate than those reported in Fig. 14.

However, Fig. 18(a) still shows similar identified values for all the local damage conditions, and Fig. 18(b) correctly reports an increasing trend due to the growing damage entity.

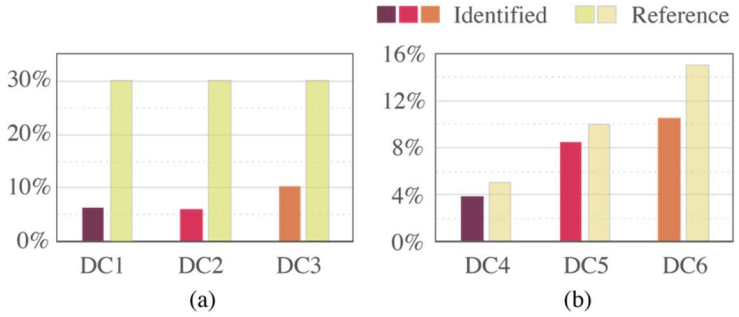

Fig. 18 – Identified damage entity in the noisy environment: (a) Local damage; (b) Diffuse damage.

5. CONCLUSIONS

In this paper, a novel approach for structural health monitoring of simply-supported RC viaducts has been presented, capable of identifying in a simple and integrated fashion both dynamic and quasi-static parameters. Specifically, the modal assurance distribution (MAD) has shown to be suitable to extract sparse estimates of modal parameters from structures subjected to traffic excitation using clustered wavelet bandpass filters. Accurate identification of mode shapes and natural frequencies of three viaducts has been achieved. Besides, quasi-static features enable a dense description of the structural behavior using few accelerometers. The curvature influence line obtained from low-frequency signal components extracted through an additional lowpass wavelet filter is indeed representative of the curvature of the structure subjected to a vertical force applied at the instrumented location. Exploiting this fact, a curvature-based damage-sensitive feature has been proposed, avoiding however the approximations introduced by traditional techniques that involve double differentiation of identified mode shapes. A damage index defined as the difference of the curvature influence lines has shown the ability to localize damage with good accuracy using a sparse sensor network of accelerometers. Furthermore, the proposed index is representative of the damage entity and does not require any knowledge about structural masses or the use of finite element models. The results obtained from a numerical case study have shown that noise can affect the outcome of the identification procedure when using extremely sparse sensor networks (e.g., down to only one sensor). However, the cumulative difference function obtained by subtracting the inspection influence line from the baseline in multiple sensing locations considerably improves the accuracy of damage localization. Moreover, information obtained from modal features can help to discard peaks of the damage index generated by dynamic effects and thus not related to actual damage. The proposed procedure has provided promising results, proving particularly appealing for applications employing low-cost sparse sensing solutions for structural health monitoring at a territorial level.

ACKNOWLEDGEMENTS

The authors would kindly acknowledge the research group of Prof. Rocco Alaggio and, in particular, Dr. Angelo Aloisio (Univeristy of L'Aquila, Italy) for having shared the experimental data of the A24 viaducts.

APPENDIX A: FOURIER TRANSFORM OF THE QUASI-STATIC CONTRIBUTION

Substituting $T = 2l/v$ in Eq. (10), it is possible to write $l_m(t)$ as

$$l_m(t) = \sin\left(\frac{m\pi v t}{l}\right)\prod\left(\frac{t - T/4}{T/2}\right) \tag{A.1}$$

where T is the period of the sine function in the above equation when $m = 1$, i.e., twice the time a passing car with a velocity equal to v takes to enter and leave the bridge span. Thanks to the frequency shift property, the Fourier transform of $l_m(t)$ can be written as

$$L_m(f) = \mathcal{F}[l_m(t)] = \mathcal{F}[l'_m(t)]e^{-j\frac{\pi l}{v}f} \tag{A.2}$$

where the shifted function $l'_m(t)$ reads:

$$l'_m(t) = \cos\left(\frac{m\pi v}{l}t + \frac{m-1}{2}\pi\right)\prod\left(\frac{t}{T/2}\right) \tag{A.3}$$

The modulation theorem of Fourier transform can thus be employed, obtaining:

$$\begin{aligned}\mathcal{F}[l'_m(t)] &= \frac{le^{j\frac{m-1}{2}\pi}}{2v}\operatorname{sinc}\left(\frac{l}{v}f - \frac{m}{2}\right) + \frac{le^{-j\frac{m-1}{2}\pi}}{2v}\operatorname{sinc}\left(\frac{l}{v}f + \frac{m}{2}\right) = \\ &= \frac{l}{2v}\left[e^{j\frac{m-1}{2}\pi}\frac{\sin\left(\frac{\pi l}{v}f - \frac{m\pi}{2}\right)}{\frac{\pi l}{v}f - \frac{m\pi}{2}} + e^{-j\frac{m-1}{2}\pi}\frac{\sin\left(\frac{\pi l}{v}f + \frac{m\pi}{2}\right)}{\frac{\pi l}{v}f + \frac{m\pi}{2}}\right]\end{aligned} \tag{A.4}$$

It should be noted that:

$$e^{j\frac{m-1}{2}\pi}\sin\left(\frac{\pi l}{v}f - \frac{m\pi}{2}\right) + e^{-j\frac{m-1}{2}\pi}\sin\left(\frac{\pi l}{v}f + \frac{m\pi}{2}\right) = 0 \ \ \forall m \tag{A.5}$$

$$e^{j\frac{m-1}{2}\pi}\sin\left(\frac{\pi l}{v}f - \frac{m\pi}{2}\right) - e^{-j\frac{m-1}{2}\pi}\sin\left(\frac{\pi l}{v}f + \frac{m\pi}{2}\right) = 2e^{j\frac{m-1}{2}\pi}\sin\left(\frac{\pi l}{v}f - \frac{m\pi}{2}\right) \ \ \forall m \tag{A.6}$$

Therefore, Eq. (A.4) simplifies in:

$$\mathcal{F}[l'_m(t)] = \frac{le^{j\frac{m-1}{2}\pi}}{v\left(\frac{\pi^2 l^2}{v^2}f^2 - \frac{m^2\pi^2}{4}\right)}\sin\left(\frac{\pi l}{v}f - \frac{m}{2}\right) \tag{A.7}$$

The result shown in Eq. (14) can thus be obtained by substituting Eq. (A.7) into Eq. (A.2).

REFERENCES

[1] H. Raiffa, R. Schlaifer, Applied Statistical Decision Theory, Wiley, 1961.

[2] P.F. Giordano, M.P. Limongelli, The value of structural health monitoring in seismic emergency management of bridges, Struct. Infrastruct. Eng. (In press) (2020).

[3] P.F. Giordano, L.J. Prendergast, M.P. Limongelli, A framework for assessing the value of information for health monitoring of scoured bridges, J. Civ. Struct. Heal. Monit. 10 (2020) 485–496. https://doi.org/10.1007/s13349-020-00398-0.
[4] J. Long, O. Büyüköztürk, A power optimised and reprogrammable system for smart wireless vibration monitoring, Struct. Control Heal. Monit. 27 (2020). https://doi.org/10.1002/stc.2468.
[5] S. Quqa, L. Landi, P.P. Diotallevi, Instantaneous modal identification under varying structural characteristics: A decentralized algorithm, Mech. Syst. Signal Process. 142 (2020) 106750. https://doi.org/10.1016/j.ymssp.2020.106750.
[6] S. Quqa, L. Landi, P.P. Diotallevi, Modal assurance distribution of multivariate signals for modal identification of time-varying dynamic systems, Mech. Syst. Signal Process. 148 (2021) 107136. https://doi.org/10.1016/j.ymssp.2020.107136.
[7] S. Quqa, L. Landi, P.P. Diotallevi, Seismic structural health monitoring using the modal assurance distribution, Earthq. Eng. Struct. Dyn. (2021) eqe.3451. https://doi.org/10.1002/eqe.3451.
[8] R. Brincker, C.E. Ventura, Introduction to Operational Modal Analysis, John Wiley and Sons, Ltd, 2015. https://doi.org/10.1002/9781118535141.
[9] A. Aloisio, R. Alaggio, M. Fragiacomo, Time-domain identification of the elastic modulus of simply supported box girders under moving loads: Method and full-scale validation, Eng. Struct. 215 (2020). https://doi.org/10.1016/j.engstruct.2020.110619.
[10] M.A. Khan, D.P. McCrum, L.J. Prendergast, E.J. OBrien, P.C. Fitzgerald, C.W. Kim, Laboratory investigation of a bridge scour monitoring method using decentralized modal analysis, Struct. Heal. Monit. (2021). https://doi.org/10.1177/1475921720985122.
[11] A. Malekjafarian, P.J. McGetrick, E.J. Obrien, A review of indirect bridge monitoring using passing vehicles, Shock Vib. 2015 (2015). https://doi.org/10.1155/2015/286139.
[12] Y.B. Yang, C.W. Lin, J.D. Yau, Extracting bridge frequencies from the dynamic response of a passing vehicle, J. Sound Vib. 272 (2004) 471–493. https://doi.org/10.1016/S0022-460X(03)00378-X.
[13] A. González, E.J. Obrien, P.J. McGetrick, Identification of damping in a bridge using a moving instrumented vehicle, J. Sound Vib. 331 (2012) 4115–4131. https://doi.org/10.1016/j.jsv.2012.04.019.
[14] A. Aloisio, R. Alaggio, M. Fragiacomo, Bending Stiffness Identification of Simply Supported Girders using an Instrumented Vehicle: Full Scale Tests, Sensitivity Analysis, and Discussion, J. Bridg. Eng. 26 (2021) 04020115. https://doi.org/10.1061/(asce)be.1943-5592.0001654.
[15] R. Zaurin, F.N. Catbas, Structural health monitoring using video stream, influence lines, and statistical analysis, Struct. Heal. Monit. 10 (2011) 309–332. https://doi.org/10.1177/1475921710373290.
[16] B. Chen, X. Wang, D. Sun, X. Xie, Integrated system of structural health monitoring and intelligent management for a cable-stayed bridge, Sci. World J. 2014 (2014). https://doi.org/10.1155/2014/689471.
[17] J. Kim, J.P. Lynch, J.J. Lee, C.G. Lee, Truck-based mobile wireless sensor networks for the experimental observation of vehicle-bridge interaction, Smart Mater. Struct. 20 (2011). https://doi.org/10.1088/0964-1726/20/6/065009.
[18] W.Y. He, W.X. Ren, S. Zhu, Damage detection of beam structures using quasi-static moving load induced displacement response, Eng. Struct. 145 (2017) 70–82. https://doi.org/10.1016/j.engstruct.2017.05.009.
[19] F. Cavadas, I.F.C. Smith, J. Figueiras, Damage detection using data-driven methods applied to moving-load responses, Mech. Syst. Signal Process. 39 (2013) 409–425. https://doi.org/10.1016/j.ymssp.2013.02.019.
[20] G.T. Frøseth, A. Rønnquist, D. Cantero, O. Øiseth, Influence line extraction by deconvolution in the frequency domain, Comput. Struct. 189 (2017) 21–30. https://doi.org/10.1016/j.compstruc.2017.04.014.

[21] X. Zheng, D.-H. Yang, T.-H. Yi, H.-N. Li, Z.-W. Chen, Bridge Influence Line Identification Based on Regularized Least-Squares QR Decomposition Method, J. Bridg. Eng. 24 (2019) 06019004. https://doi.org/10.1061/(asce)be.1943-5592.0001458.
[22] X. Zheng, D.H. Yang, T.H. Yi, H.N. Li, Development of bridge influence line identification methods based on direct measurement data: A comprehensive review and comparison, Eng. Struct. 198 (2019). https://doi.org/10.1016/j.engstruct.2019.109539.
[23] D. Hester, J. Brownjohn, F. Huseynov, E. Obrien, A. Gonzalez, M. Casero, Identifying damage in a bridge by analysing rotation response to a moving load, Struct. Infrastruct. Eng. 16 (2020) 1050–1065. https://doi.org/10.1080/15732479.2019.1680710.
[24] B. Heitner, F. Schoefs, E.J. OBrien, A. Žnidarič, T. Yalamas, Using the unit influence line of a bridge to track changes in its condition, J. Civ. Struct. Heal. Monit. 10 (2020) 667–678. https://doi.org/10.1007/s13349-020-00410-7.
[25] Z.-W. Chen, S. Zhu, Y.-L. Xu, Q. Li, Q.-L. Cai, Damage Detection in Long Suspension Bridges Using Stress Influence Lines, J. Bridg. Eng. 20 (2015) 05014013. https://doi.org/10.1061/(ASCE)BE.1943-5592.0000681.
[26] A. Žnidarič, J. Kalin, Using bridge weigh-in-motion systems to monitor single-span bridge influence lines, J. Civ. Struct. Heal. Monit. 10 (2020) 743–756. https://doi.org/10.1007/s13349-020-00407-2.
[27] E. Parloo, P. Verboven, P. Guillaume, M. Van Overmeire, Sensitivity-based operational mode shape normalisation, Mech. Syst. Signal Process. 16 (2002) 757–767. https://doi.org/10.1006/mssp.2002.1498.
[28] P.G. Bakir, E. Reynders, G. De Roeck, Sensitivity-based finite element model updating using constrained optimization with a trust region algorithm, J. Sound Vib. 305 (2007) 211–225. https://doi.org/10.1016/j.jsv.2007.03.044.
[29] A. Aloisio, R. Alaggio, M. Fragiacomo, Dynamic identification and model updating of full-scale concrete box girders based on the experimental torsional response, Constr. Build. Mater. 264 (2020). https://doi.org/10.1016/j.conbuildmat.2020.120146.
[30] A. Aloisio, D.P. Pasca, R. Alaggio, M. Fragiacomo, Bayesian estimate of the elastic modulus of concrete box girders from dynamic identification: a statistical framework for the A24 motorway in Italy, Struct. Infrastruct. Eng. (2020). https://doi.org/10.1080/15732479.2020.1819343.
[31] C.R. Farrar, K. Worden, Structural Health Monitoring: A Machine Learning Perspective, Struct. Heal. Monit. A Mach. Learn. Perspect. (2012). https://doi.org/10.1002/9781118443118.
[32] G. Kerschen, K. Worden, A.F. Vakakis, J.C. Golinval, Past, present and future of nonlinear system identification in structural dynamics, Mech. Syst. Signal Process. 20 (2006) 505–592. https://doi.org/10.1016/j.ymssp.2005.04.008.
[33] L. Frýba, Vibration of solids and structures under moving loads, Vib. Solids Struct. under Mov. Loads. (1972). https://doi.org/10.1007/978-94-011-9685-7.
[34] X. Zheng, D.H. Yang, T.H. Yi, H.N. Li, Bridge influence line identification from structural dynamic responses induced by a high-speed vehicle, Struct. Control Heal. Monit. 27 (2020). https://doi.org/10.1002/stc.2544.
[35] M. Ester, H.P. Kriegel, J. Sander, X. Xu, Density-Connected Sets and their Application for Trend Detection in Spatial Databases, Proc. 3rd Int. Conf. Knowl. Discov. Data Mining, Newport Beach, CA. (1997) 10–15.
[36] R. Brincker, L. Zhang, P. Andersen, Modal identification of output-only systems using frequency domain decomposition, Smart Mater. Struct. 10 (2001) 441–445. https://doi.org/10.1088/0964-1726/10/3/303.